Radiative corrections to light thermal pseudo-Dirac dark matter

Gopolang Mohlabeng,[1,2,*] Adreja Mondol,[1,†] and Tim M. P. Tait[1,‡]

[1]*Department of Physics and Astronomy, University of California, Irvine, California 92697, USA*
[2]*Department of Physics, Simon Fraser University, Burnaby, British Columbia V5A 1S6, Canada*

(Received 28 May 2024; accepted 30 January 2025; published 6 March 2025)

Light thermal dark matter has emerged as an attractive theoretical possibility and a promising target for discovery at experiments in the near future. Such scenarios generically invoke mediators with very small couplings to the Standard Model, but with moderately strong couplings within the dark sector, calling into question theoretical estimates based on the lowest order of perturbation theory. As an example, we focus on a scenario in which (pseudo-)Dirac fermion dark matter is connected to the Standard Model via a dark photon charged under a new $U(1)'$ extension of the standard model, and we investigate the impact of the next-to-leading order corrections to annihilation and scattering. We find that radiative corrections can significantly impact model predictions for the relic density and scattering cross section, depending on the strength of the dark sector coupling and ratio of the dark matter to mediator mass. We also show why factorization into the yield parameter Y typically presented in literature leads to imprecision. Our results are necessary to accurately map experimental searches into the model parameter space and assess their ability to reach thermal production targets.

DOI: 10.1103/PhysRevD.111.056003

I. INTRODUCTION

Of all of the viable scenarios of dark matter (DM), one of the most compelling is that of particles that are in thermal equilibrium with the Standard Model (SM) bath in the early Universe. DM with a thermal history is very well motivated because it not only provides a feasible prediction for large nongravitational interactions between dark and ordinary matter, but it is also highly predictive in nature, leading to clear targets for experimental searches. Generically, after the DM has frozen out and its relic density set, it maintains the same interaction strength with the SM today, predicting that it is likely to be observable at a variety of experiments on Earth [1]. A canonical example is that of weakly interacting massive particles (WIMPs), a class of heavy ($\sim$ GeV $-$ TeV scale) particles that interact with the SM through a roughly electroweak strength force [2,3].

However, despite decades of search, heavy ($\gtrsim$GeV) WIMPs are yet to be discovered and their parameter space has become tightly constrained [3]. This lack of a clear signal has motivated searches for other visions of DM, including models with masses in the MeV to GeV regime interacting with the SM via new undiscovered forces. While this class of DM is no longer a WIMP in the traditional sense, it can still be in equilibrium at early times and thus represents a thermal target. It is a very attractive prospect as it may provide a road map to a wide and rich dark sector. The possibilities of simplified DM models are vast. However, one of the most appealing scenarios is that of DM interacting with the SM through a new vector boson, often referred to as a dark photon, corresponding to a $U(1)'$ extension of the SM [4–6].

Thermal sub-GeV DM, through a dark photon portal is very well motivated and has been the subject of much exploration in the literature. In this scenario, MeV to GeV mass DM can be produced and detected at a variety of current and near-future low energy accelerator experiments [7–28]. Moreover, ambient DM in the Solar System can scatter with electrons and nucleons in small scale direct detection experiments with low energy recoil thresholds [29–31]. In addition, accelerator and underground detector probes are well complemented by astrophysical and cosmological constraints [32–37]. All together, these probes make for an exciting experimental program that shows promise for discovering light thermal DM in the near future.

As an illustrative model, we focus on pseudo-Dirac dark matter interacting with the SM via a dark photon mediator. While we present results for the case in which the dark photon's interactions with the SM arise entirely via kinetic mixing with the hypercharge boson, our results are actually

*Contact author: gmohlabe@sfu.ca
†Contact author: amondol@uci.edu
‡Contact author: ttait@uci.edu

more general and apply to any theory in which a pseudo-Dirac dark matter particle interacts with a vector mediator whose interactions with the SM are much weaker than those with the dark matter itself. Current experimental constraints and projections on this model that target the dark matter thermal relic abundance focus on a dark sector coupling α_D that is stronger than the QCD coupling at the electroweak scale. As a result, the dark sector is strongly coupled and relatively large corrections from higher orders of perturbation theory are expected. In this work, we compute the next-to-leading (NLO) order corrections on both the thermal annihilation and late time-scattering processes with electrons. We focus on the NLO corrections at $\mathcal{O}(\alpha_D)$ and neglect the presumably negligible higher order corrections from the tiny kinetic mixing.

We find that the NLO corrections can be as large as $\mathcal{O}(10\%)$ for parameters typically discussed in the literature, and are thus necessary to take into account when precisely mapping experimental searches into the parameter space, and when comparing them with thermal production milestones that serve as a prime target for a currently growing intensity frontier program. It is worth pointing out that various theoretical constraints on this model resulting from its strong coupling have been considered in the literature, e.g., from the running of the dark sector coupling and the breakdown of perturbation theory [38,39].

The rest of this article is organized as follows: In Sec. II we describe the reference model, Sec. III is devoted to a full description of the thermal annihilation cross section, including both leading and next-to-leading order (NLO) processes. We compute the scattering cross sections with electrons relevant for direct detection searches in Sec. IV. Finally we conclude in Sec. V. The appendices provide some technical details related to the counterterms in the on-shell renormalization scheme.

II. PSEUDO-DIRAC DARK MATTER

The basic module we consider consists of two Weyl fermions which play the role of dark matter and are paired by a Dirac mass, m_χ. These fermions are neutral under the SM gauge groups but have equal and opposite charge ± 1 under a gauged dark $\mathrm{U}(1)'$, with corresponding gauge boson A'_μ. The $\mathrm{U}(1)'$ symmetry is spontaneously broken by the vacuum expectation value of a dark scalar ϕ, generating a mass for A'_μ and [assuming the ϕ charge under $\mathrm{U}(1)'$ is chosen appropriately] Majorana masses for the two Weyl fermions. We further assume that there is kinetic mixing between the dark photon and the SM hypercharge interaction, induced by unspecified UV physics.

In the mass basis, linear combinations of the original Weyl fermions appear as Majorana fermions, with their mixing determined by the Majorana masses and m_χ. We follow the standard assumptions in the literature that the Majorana masses are much smaller than m_χ. In this limit, the mass splitting between the two Majorana states goes to zero, and the pair can be approximately described as a single "pseudo-Dirac" state χ. Strictly speaking, this limit is experimentally ruled out by bounds from the cosmic microwave background [22,40]. However, relatively small splittings can ameliorate these bounds [22], and the pseudo-Dirac limit is a reasonable approximation to viable models over much of the parameter space.

Putting these ingredients together, the resulting theory is described by the SM Lagrangian supplemented by terms describing the dark matter, mediator, and dark Higgs:

$$\mathcal{L}_{\mathrm{DM}} = i\bar{\chi}\gamma^\mu D_\mu \chi - m_\chi \bar{\chi}\chi - \frac{1}{4}X_{\mu\nu}X^{\mu\nu} + \frac{m_{A'}^2}{2}A'_\mu A'^\mu + \frac{\varepsilon}{2}X^{\mu\nu}B_{\mu\nu} + |D_\mu\phi|^2 - V(\phi), \tag{1}$$

where χ is a Dirac fermion packaging both of the original Weyl fermions in the limit of zero mass splitting (and thus including both the dark matter and its heavier partner when the mass splitting is taken into account). $D_\mu \equiv \partial_\mu - ig_D q_{A'} A'_\mu$ is the covariant derivative for field of $\mathrm{U}(1)'$ charge $q_{A'}$, $X_{\mu\nu}$ and $B_{\mu\nu}$ are the field strengths for the $\mathrm{U}(1)'$ and SM hypercharge bosons, respectively, and ε characterizes the strength of the kinetic mixing. We normalize $q_{A'} = 1$ from here on for χ. After symmetry breaking, the scalar field acquires a vacuum expectation value (VEV) v_ϕ and can be parametrized in the unitary gauge as $\phi \to (v_\phi + H_D)/\sqrt{2}$, where H_D is the dark Higgs boson.

Diagonalizing the interactions and assuming $m_{A'} \ll M_Z$, the resulting theory contains a dark photon A' interacting with coupling strength g_D with the DM, χ and strength $\varepsilon Q_f e$ with SM fields of electric charge Q_f. The dark photon mass is given by $m_{A'} = q_\phi g_D v_\phi$, with q_ϕ the charge of the dark scalar. We will assume $q_\phi = 2$ such that the dark Higgs can have interactions with the DM Weyl fermions, allowing its VEV to contribute to their Majorana masses. For simplicity, we assume that the mixing between ϕ and the SM Higgs is negligible. The mixing parameter is important when considering the phenomenology of H_D, but does not play an important role in dark matter annihilation at NLO.

III. THERMAL FREEZE-OUT

For $m_\chi \leq m_{A'}$, annihilation of $\bar{\chi}\chi$ is predominantly into pairs of SM fermions,

$$\chi(p_a) + \bar{\chi}(p_b) \to f(p_1) + \bar{f}(p_2),$$

where $p_{a,b}$ label the incoming DM and $p_{1,2}$ the outgoing final state fermion momenta. This cross section controls both the cosmological relic abundance via freeze-out and the prospects for indirect detection today. Both processes take place for dark matter with typically nonrelativistic velocity v and can be approximated by the leading (s-wave)

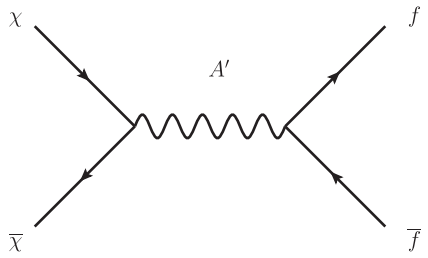

FIG. 1. Tree-level Feynman diagram for DM annihilation into SM fermions.

term in the expansion in v^2. The cross section is related to the matrix element via

$$\langle \sigma v \rangle = \frac{v}{64\pi s |\vec{p}_a|^2} \int_{t_0}^{t_1} dt \times \overline{|\mathcal{M}|^2}, \tag{2}$$

where $\overline{|\mathcal{M}|^2}$ is the matrix element, summed/averaged over final/initial polarization states, and $s \equiv (p_a + p_b)^2$ and $t \equiv (p_a - p_1)^2$ are the usual Mandelstam variables. In the nonrelativistic ($v \to 0$) limit $s \simeq 4m_\chi^2 + m_\chi^2 v^2$, $|\vec{p}_a| \simeq m_\chi v/2$, and $t_{0,1} \simeq m_f^2 - m_\chi^2 \mp m_\chi^2 \sqrt{1 - m_f^2/m_\chi^2}$.

For dark matter masses below $\lesssim$GeV, the annihilation rate into hadrons may be inferred by making use of the fact that A' couples to the same electromagnetic current as the photon. Thus, the effective cross section for annihilation into hadrons at a given center-of-mass energy can be related to the ratio R measured in e^+e^- reactions [41]:

$$R(s) = \frac{\sigma(e^+e^- \to \text{hadrons})}{\sigma(e^+e^- \to \mu^+\mu^-)}, \tag{3}$$

at a given center-of-mass energy $\sqrt{s}$. The cross section for $\chi\bar{\chi}$ to annihilate into hadrons is thus

$$\sigma(\chi\bar{\chi} \to \text{hadrons}) = \sigma(\chi\bar{\chi} \to \mu^+\mu^-) \times R(4m_\chi^2).$$

A. Tree-level annihilation

At tree level, the annihilation into SM fermions proceeds via s-channel exchange of the A' (see Fig. 1). The leading order matrix element $\overline{|\mathcal{M}|^2}_{\text{LO}}$ is given by

$$16\pi^2 \alpha \alpha_D \varepsilon^2 Q_f^2 \times \frac{(D-2)s^2 + 4(m_f^2 + m_\chi^2)^2 + (4s - 8m_f^2 - 8m_\chi^2)t + 4t^2}{(s - m_{A'}^2)^2 + \Gamma_{A'}^2 m_{A'}^2}, \tag{4}$$

where $D \equiv 4 - \epsilon$ is the dimension of space-time, $\alpha_D = g_D^2/4\pi$, $\alpha = e^2/4\pi$, and $\Gamma_{A'}$ is the width of the dark photon, given by

$$\begin{aligned}\Gamma_{A'} = {} & \Gamma(A' \to \chi\bar{\chi})\Theta(m_{A'} - 2m_\chi) \\ & + \Gamma(A' \to e^+e^-)\Theta(m_{A'} - 2m_e) \\ & + \Gamma(A' \to \mu^+\mu^-)\Theta(m_{A'} - 2m_\mu) \\ & + \Gamma(A' \to \mu^+\mu^-)R(m_{A'}^2)\Theta(m_{A'} - 2m_\pi).\end{aligned} \tag{5}$$

Here,

$$\Gamma(A' \to \chi\bar{\chi}) = \frac{\alpha_D}{3} m_{A'} \left(1 + \frac{2m_\chi^2}{m_{A'}^2}\right) \sqrt{1 - \frac{4m_\chi^2}{m_{A'}^2}}, \tag{6}$$

$$\Gamma(A' \to f\bar{f}) = \frac{\alpha Q_f^2}{3} \varepsilon^2 m_{A'} \left(1 + \frac{2m_f^2}{m_{A'}^2}\right) \sqrt{1 - \frac{4m_f^2}{m_{A'}^2}}, \tag{7}$$

are the partial decay widths into DM and SM fermions, respectively. For much of the parameter space of interest, $m_{A'} \geq 2m_\chi$ and $\varepsilon \ll 1$, leading to $\Gamma_{A'} \simeq \Gamma(A' \to \chi\bar{\chi})$.

In the nonrelativistic limit, the thermally averaged tree-level cross section is

$$\langle \sigma v \rangle_{\text{LO}} = \frac{8\pi\alpha\alpha_D Q_f^2 \varepsilon^2 (2m_\chi^2 + m_f^2)}{(4m_\chi^2 - m_{A'}^2)^2 + \Gamma_{A'}^2 m_{A'}^2} \sqrt{1 - \frac{m_f^2}{m_\chi^2}}, \tag{8}$$

which agrees with Refs. [10,42] in the $m_f \to 0$ limit.

In the literature, it is common to factor out the combination $Y \equiv \varepsilon^2 \alpha_D (m_\chi/m_{A'})^4$ which controls tree-level annihilation in the $m_{A'} \gg m_\chi$ limit. This leads to imprecision. First, the relevant parameter space is typically $m_{A'} \simeq m_\chi$, and errors of order $m_\chi^2/m_{A'}^2$ are typically substantial. Second, the higher order corrections to the annihilation rate considered below are $\mathcal{O}(\alpha_D^2)$, and thus do not factorize in the same way. And finally, various constraints and experimental prospects do not themselves factorize in the same way, which can make comparison using it as a parameter rather misleading. For this reason, we focus on the direct model parameters $\{\varepsilon, \alpha_D, m_\chi, m_{A'}\}$ in our analyses.

B. NLO corrections

At $\mathcal{O}(\alpha_D^2)$, the annihilation cross section receives virtual corrections in the form of self-energy corrections to the dark photon propagator (these include diagrams with fermions and the dark Higgs in the loop) and incoming dark matter wave functions as well as a correction to the $A' - \chi - \bar{\chi}$ vertex (see Fig. 2). In the regime of $m_A' \geq 2m_\chi$, an additional emitted A' would always be off-shell, leading the real emission corrections to be effectively higher order in ε such that they can be safely neglected. The $\mathcal{O}(\alpha_D^2)$ correction to the annihilation process is given by the interference between the leading order and next-to-leading order matrix elements in the nonrelativistic limit, summed and averaged over the final and initial polarizations,

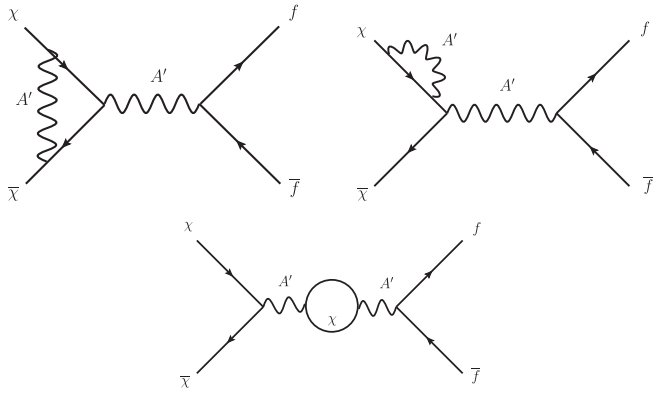

FIG. 2. Representative Feynman diagrams for the one-loop corrections to $\chi\bar{\chi} \to f\bar{f}$.

$$\overline{\delta\mathcal{M}^2} = 2\mathrm{Re}\{\overline{\mathcal{M}^*_{\mathrm{LO}} \times \mathcal{M}_{\mathrm{NLO}}}\}. \tag{9}$$

We compute the one loop diagrams in the nonrelativistic limit with the aid of FeynCalc [43], interfere them with the LO matrix elements, and reduce the resulting expressions via the Passarino-Veltman procedure [44] to scalar integrals which we evaluate numerically using LoopTools [45]. We cross-checked our results by hand as well as by using Package-X [46]. We find that the ultraviolet divergences cancel between the DM wave function corrections (see Appendix A) and the vertex correction, as is expected based on the analogue of the Ward identity for U(1)′. UV divergences in the one-loop correction to the dark photon propagator cancel against the $\delta Z_{A'}$ and $\delta m^2_{A'}$ counterterms, renormalized in the on-shell scheme (see Appendix B for details), resulting in a final expression that is finite.

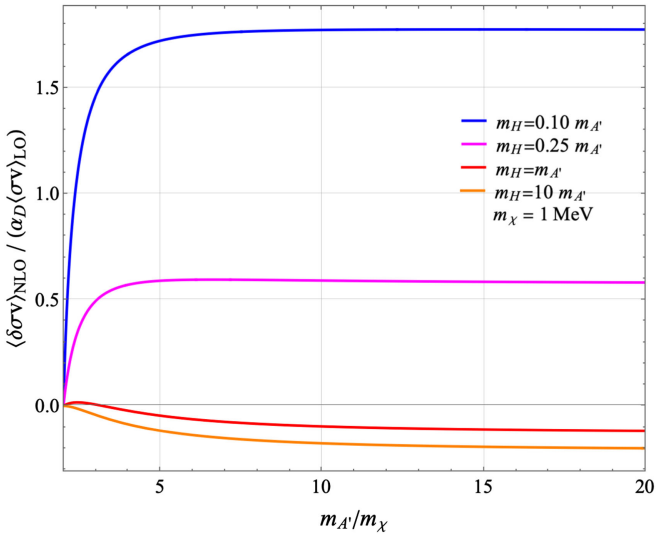

FIG. 3. The ratio $\langle\delta\sigma v\rangle_{\mathrm{NLO}}/(\alpha_D\langle\sigma v\rangle_{\mathrm{LO}})$ as a function of $m_{A'}/m_\chi$, for $m_\chi = 1$ MeV and for different ratios of $m_H/m_{A'} = 0.1, 0.25, 1$, and 10, represented by the blue, magenta, red, and orange lines, respectively.

The resulting correction to the annihilation cross section from diagrams without a dark Higgs is expressed as

$$\begin{aligned}\langle\delta\sigma v\rangle^{\mathrm{DM}}_{\mathrm{NLO}} = &-\frac{\alpha_D\langle\sigma v\rangle_{\mathrm{LO}}}{3\pi} - \frac{\alpha_D\langle\sigma v\rangle_{\mathrm{LO}}}{6\pi m_\chi^2(4m_\chi^2 - m_{A'}^2)}\{-2(m_{A'}^2 - 4m_\chi^2)(m_\chi^2(m_{A'}^2 + 2m_\chi^2)(2B_0'(m_{A'}^2; m_\chi^2, m_\chi^2) + 3B_0'(m_\chi^2; m_{A'}^2, m_\chi^2)) \\ &+ A_0(m_{A'}^2) - A_0(m_\chi^2)) + 24m_\chi^4 B_0(m_{A'}^2; m_\chi^2, m_\chi^2) + (m_{A'}^4 - 14m_{A'}^2 m_\chi^2 + 40m_\chi^4)B_0(m_\chi^2; m_{A'}^2, m_\chi^2) \\ &+ (m_{A'}^4 + 4m_{A'}^2 m_\chi^2 - 56m_\chi^4)B_0(4m_\chi^2; m_\chi^2, m_\chi^2) \\ &+ (m_{A'}^6 + 4m_{A'}^4 m_\chi^2 - 20m_{A'}^2 m_\chi^4 - 48m_\chi^6)C_0(m_\chi^2, m_\chi^2, 4m_\chi^2; m_\chi^2, m_{A'}^2, m_\chi^2)\},\end{aligned} \tag{10}$$

where A_0, B_0, and C_0 are scalar integral functions, and B_0' is the derivative of B_0 with respect to its first argument. The contribution from the one-loop correction involving the dark Higgs is

$$\begin{aligned}\langle\delta\sigma v\rangle^{\mathrm{Higgs}}_{\mathrm{NLO}} = &\frac{\langle\sigma v\rangle_{\mathrm{LO}}\alpha_D q_\phi^2}{24\pi m_{A'}^4 m_\chi^2(m_{A'}^2 - 4m_\chi^2)}\{B_0(m_{A'}^2; m_{A'}^2, m_H^2)[-8m_\chi^2(6m_{A'}^6 - 3m_{A'}^4 m_H^2 + m_{A'}^2(m_H^4 + 4m_H^2 m_\chi^2) - 2m_H^4 m_\chi^2)] \\ &+ B_0(4m_\chi^2; m_{A'}^2, m_H^2)[m_{A'}^4(m_{A'}^4 - 2m_{A'}^2(m_H^2 - 20m_\chi^2) + (m_H^2 - 4m_\chi^2)^2)] \\ &+ B_0'(m_{A'}^2; m_{A'}^2, m_H^2)[4m_{A'}^2 m_\chi^2(12m_{A'}^4 - 4m_{A'}^2 m_H^2 + m_H^4)(m_{A'}^2 - 4m_\chi^2)] \\ &+ (m_{A'}^2 - m_H^2)(m_{A'}^2 - 4m_\chi^2)^2[A_0(m_H^2) - A_0(m_{A'}^2)]\}.\end{aligned} \tag{11}$$

The full annihilation cross section to $\mathcal{O}(\alpha_D^2)$ is

$$\langle\sigma v\rangle = \langle\sigma v\rangle_{\mathrm{LO}} + \langle\delta\sigma v\rangle^{\mathrm{DM}}_{\mathrm{NLO}} + \langle\delta\sigma v\rangle^{\mathrm{Higgs}}_{\mathrm{NLO}} + \mathcal{O}(\alpha_D^3). \tag{12}$$

The impact of the one-loop correction can be summarized by the quantity $\langle\delta\sigma v\rangle_{\mathrm{NLO}}/(\alpha_D\langle\sigma v\rangle_{\mathrm{LO}})$, which characterizes the relative change compared to the leading order cross section with the α_D dependence scaled out. In Fig. 3, we plot this ratio as a function of the ratio of $m_{A'}/m_\chi$, for $m_\chi = 1$ MeV for different values of $m_H/m_{A'}$. As illustrated in the figure, in the limit of large dark Higgs mass, the net effect of the NLO corrections is to reduce the cross section by a modest amount. As $m_H/m_{A'}$ decreases, the NLO effect is to increase the total annihilation cross section significantly. This trend

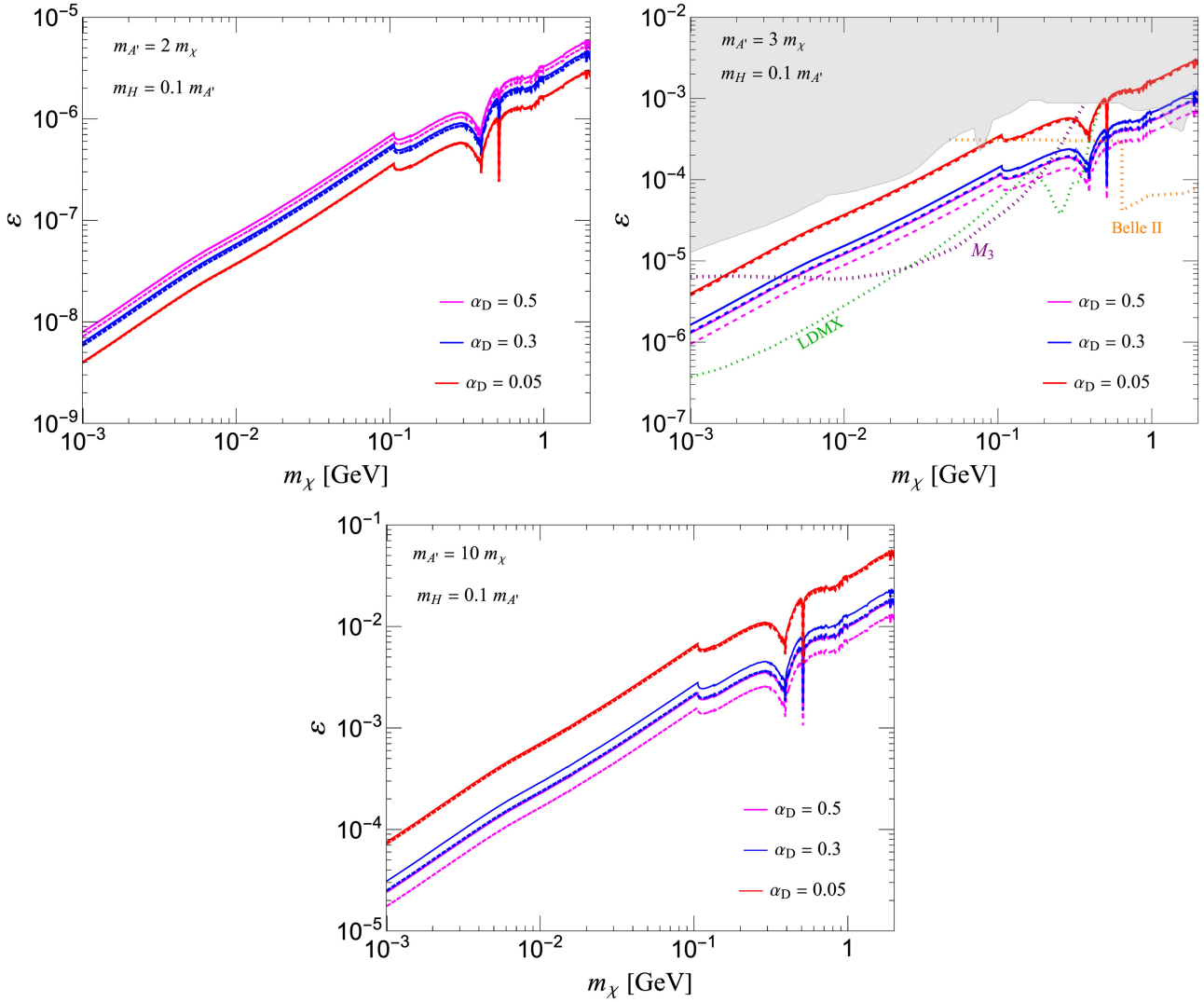

FIG. 4. Value of ε producing the observed relic abundance of dark matter as a function of m_χ, for $\alpha_D = 0.05$, 0.3, and 0.5 (red, blue, and magenta lines, respectively) based on LO only (solid lines) and NLO + LO (dashed lines) cross sections and for the indicated value of $m_{A'}/m_\chi$ and $m_H/m_{A'}$ on each panel. For the $m_{A'} = 3m_\chi$ panel, the gray shaded regions are the exclusions from past accelerator experiments, and the green, purple, and orange dotted lines are projections from the upcoming LDMX, M_3 and Belle II experiments, respectively [24]. We show the experimental constraints in the $m_{A'} = 3m_\chi$ panel, which have been extensively studied in the literature. It is worth emphasizing that there are expected to be analogous constraints on the other panels, but they require further analysis to be determined and will be addressed in future work.

saturates around $m_{A'}/m_\chi \sim 5$, after which the total cross section flattens out for very large mass ratios. We also find that, provided $m_{A'}$ and m_H are specified as a ratio to m_χ, the quantity $\langle \delta\sigma v\rangle_{\rm NLO}/(\alpha_D\langle\sigma v\rangle_{\rm LO})$ is insensitive to the mass of the dark matter over the entire range of interest, while we choose a benchmark $m_\chi = 1$ MeV, the results are identical for, e.g., $m_\chi = 1$ GeV.

C. Relic density

To compute the relic density we follow the description of Refs. [47,48] where it was pointed out that care is required in the treatment of the number of relativistic degrees of freedom as a function of temperature for sub-GeV dark matter annihilations. Hence, we solve the Boltzmann equation for the comoving number density of dark matter,

$$\frac{dY}{dx} = \frac{s\langle\sigma v\rangle}{Hx}\left[1 + \frac{1}{3}\frac{d(\ln g_s)}{d(\ln T)}\right](Y_{\rm eq}^2 - Y^2). \tag{13}$$

We refer the reader to Ref. [47] for discussion of the relevant quantities. Reference [47] presented results for the target cross section which reproduces the observed DM density only down to $m_\chi \sim 100$ MeV. To cover the relevant parameter space, we implement their formalism, reproducing their results in the regime that they covered and extend them down to ∼1 MeV DM masses.

In Fig. 4 we show plots of kinetic mixing as a function of DM mass for a few representative values of the ratio of $m_{A'}/m_\chi$ and choose a benchmark parameter point $m_H = 0.1 m_{A'}$. These plots were obtained by scanning through the kinetic mixing for each DM mass and finding the combination (ε, m_χ) resulting in the observed relic abundance $\Omega h^2 = 0.12$ [49]. Each plot shows the required kinetic mixing parameter for three different values of the dark sector coupling α_D, corresponding to the LO only (solid lines) and NLO + LO (dashed lines) computations, respectively. $m_{A'}/m_\chi = 3$ is typically chosen as a benchmark parameter point in the literature and is the most extensively studied. Hence, we show the current experimental constraints on this parameter space (a combination of both accelerator and astrophysical probes [24]) in the gray shaded region. In that panel, the green, purple, and orange dotted lines are sensitivity projections for the upcoming LDMX, M_3 and Belle II experiments, respectively. Assessing the experimental constraints on the other two panels is complex, and a thorough analysis is beyond the scope of this work. Following the trend in Fig. 3, we see in the top right panel, i.e., $m_{A'} = 2m_\chi$, the loop corrections result in not-so-significant changes in the thermal relic density lines, especially when lowering the value of the dark sector coupling constant α_D. As one increases the value of $m_{A'}/m_\chi$, we start seeing a significant change in the thermal relic line as a result of the loop corrections, especially for the large values of α_D which are often referenced in the literature, making these effects important to consider. We also note that the effect of these corrections can be even more dramatic if one further decreases the mass ratio $m_H/m_{A'}$. Finally, in order for the future experiments to correctly characterize their future signals, the significance of these results should be taken into account.

IV. DARK MATTER DIRECT DETECTION

In this section we investigate NLO corrections to light pseudo-Dirac DM scattering with the SM in direct detection experiments. Due to crossing symmetry, the corrections we consider here are described by similar diagrams as in Fig. 2. Since the dark photon kinetically mixes with the SM photon, DM can scatter universally with both leptons and nucleons. Given the tiny momentum transfers and our parameter space of interest for which $m_{A'} \gtrsim m_\chi$, the interaction can be approximated as an effective four-point fermion interaction, integrating out the mediator.

The spin averaged matrix element squared in the zero-momentum exchange limit is

$$|\overline{\mathcal{M}_{\rm EFT}}|^2 = \{|\bar{\mathcal{M}}|^2_{\rm LO} + \overline{\delta\mathcal{M}^2}\}_{t\to 0}, \tag{14}$$

where $\overline{\delta\mathcal{M}^2}$ corresponds to Eq. (9) and includes contributions from the one-loop corrections to the vertex, DM self-energy and the dark photon vacuum polarization, analogous to those represented in Fig. 2.

Given our focus on sub-GeV DM and the prospects for its detection at upcoming experiments, we restrict our attention to DM scattering with electrons. However our general computations can be extended to nucleon scattering with the incorporation of the appropriate form factors for either spin-dependent or spin-independent scattering.

The differential DM-electron scattering cross section as a function of the momentum transfer q is usually written

$$\frac{d\sigma}{dq^2} = \frac{\bar{\sigma}_e}{4\mu v^2}|F_{\rm DM}(q)|^2. \tag{15}$$

Here $\bar{\sigma}_e$ is defined as the free scattering cross section at a reference value $q = \alpha m_e$ [29,50], which typifies the momentum of an electron bound in an atom in the detector. For the DM mass range, and ratios with the mediator mass ($m_{A'}/m_\chi$) we consider in this work, $q \sim \mu v \ll m_{A'}$, and hence $F_{\rm DM}(q) \to F_{\rm DM}(q=0) \sim 1$.

Similarly to the annihilation case, the cross section for scattering with electrons up to $\mathcal{O}(\alpha_D^2)$, can be parametrized as

$$\overline{\sigma_e} = \overline{\sigma}_e^{\rm LO} + \overline{\delta\sigma_e}^{\rm NLO}_{\rm DM} + \overline{\delta\sigma_e}^{\rm NLO}_{\rm Higgs} + \mathcal{O}(\alpha_D^3). \tag{16}$$

At zero momentum transfer, the LO scattering cross section is given by [29,50]

$$\bar{\sigma}_e^{\rm LO} = \frac{16\pi\alpha\alpha_D\varepsilon^2\mu^2}{m_{A'}^4}, \tag{17}$$

where $\mu \equiv m_\chi m_e/(m_\chi + m_e)$ is the reduced mass between the DM and the electron. The $\mathcal{O}(\alpha_D^2)$ correction can be written in terms of scalar integrals as

$$\begin{aligned}\overline{\delta\sigma_e}^{\rm NLO}_{\rm DM} = \frac{\alpha_D \overline{\sigma_e}^{\rm LO}}{12\pi m_{A'}^2 m_\chi^2}\big[&-m_{A'}^2(-2m_{A'}^2 - 4m_\chi^2)\{4m_\chi^2 B_0'(m_{A'}^2; m_\chi^2, m_\chi^2) - 3(B_0(0; m_\chi^2, m_\chi^2) - B_0(m_\chi^2; m_{A'}^2, m_\chi^2)\\ &+ (m_{A'}^2 - 2m_\chi^2)C_0(0, m_\chi^2, m_\chi^2; m_\chi^2, m_\chi^2, m_{A'}^2) - 2m_\chi^2 B_0'(m_\chi^2; m_{A'}^2, m_\chi^2))\}\\ &- 16m_\chi^4(B_0(m_{A'}^2; m_\chi^2, m_\chi^2) - B_0(0; m_\chi^2, m_\chi^2))\big].\end{aligned} \tag{18}$$

The contribution to the scattering cross-section from the dark Higgs is

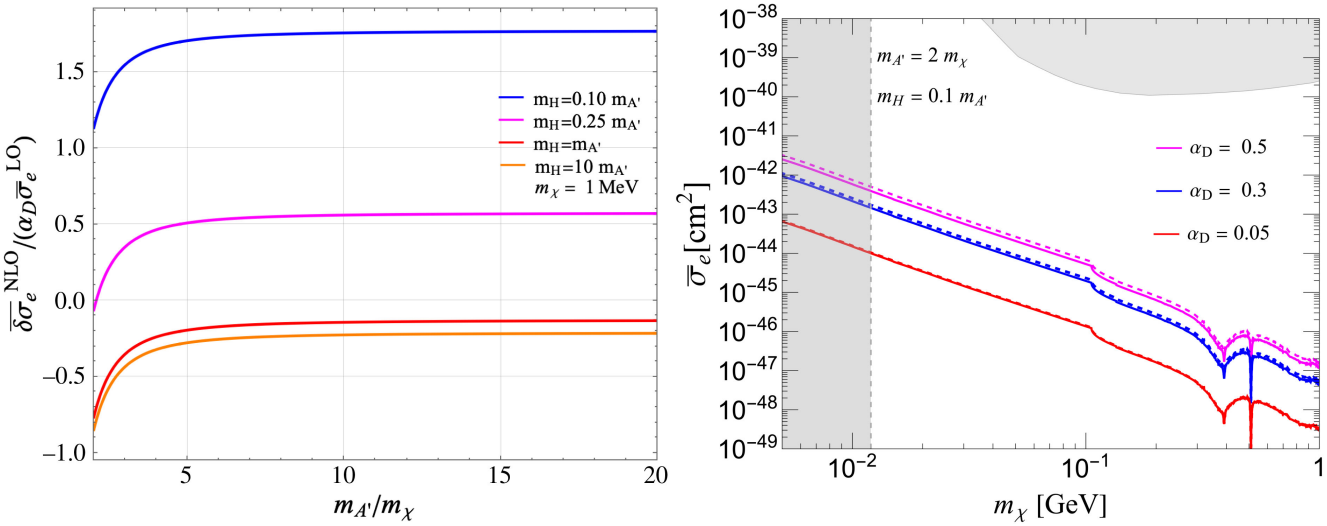

FIG. 5. Dark matter direct detection parameter space. The left panel shows the ratio of NLO to LO electron scattering cross section vs $m_{A'}/m_\chi$ ratio for $m_\chi = 1$ MeV and for $m_H/m_{A'} = 0.1$, 0.25, 1, and 10, represented by the blue, magenta, red, and orange lines, respectively. The plot for $m_\chi = 1$ GeV is identical to the left panel. The right panel shows dark matter-electron scattering cross section vs m_χ for dark matter thermal relic abundance with $\alpha_D =$, 0.05, 0.3, and 0.5, represented by the red, blue, and magenta lines, respectively, for $m_H/m_{A'} = 0.1$. We show both the LO only (solid lines) and NLO + LO (dashed lines) for the $m_{A'}/m_\chi = 2$ case. The upper gray shaded region represents the current model independent direct detection constraints from a combination of the XENON1T, PANDAX, and SENSEI experiments and the vertical gray shaded region is the constraint from $\Delta N_{\rm eff}$. All constraints were obtained from Ref. [31].

$$\overline{\delta\sigma}_{e\,\rm Higgs}^{\rm NLO} = \frac{q_\phi^2\alpha_D\overline{\sigma_e}^{\rm LO}}{6\pi m_{A'}^4(m_{A'}^2-m_H^2)}[(m_{A'}^2-m_H^2)\{m_{A'}^2((m_{A'}^2-m_H^2)^2B_0'(0;m_{A'}^2,m_H^2)+(12m_{A'}^4-4m_{A'}^2m_H^2+m_H^4)B_0'(m_{A'}^2;m_{A'}^2,m_H^2))$$
$$-2(6m_{A'}^4-3m_{A'}^2m_H^2+m_H^4)B_0(m_{A'}^2;m_{A'}^2,m_H^2)\}+2(6m_{A'}^4-3m_{A'}^2m_H^2+m_H^4)(A_0(m_{A'}^2)-\mathrm{A}_0(m_H^2))], \quad (19)$$

where we have used the identity $B_0(0;m_1^2,m_2^2) = (A_0(m_1^2) - A_0(m_2^2))/(m_1^2-m_2^2)$.

In Fig. 5, we show the direct detection constraints on the model. The left panel characterizes the importance of the one-loop correction, parametrized by the quantity $\overline{\delta\sigma}_{e\rm NLO}/(\alpha_D\bar{\sigma}_{e\rm LO})$ in terms of the ratio $m_{A'}/m_\chi$ and for different values of $m_H/m_{A'}$, similar to Fig. 3. Again, we find that this quantity is independent of the DM mass, and we choose $m_\chi = 1$ MeV for reference.

In the right panel, we show the averaged DM-electron scattering cross section vs DM mass. The red, blue, and magenta lines represent DM produced through the thermal freeze-out mechanism for benchmark choices of $\alpha_D = 0.05$, 0.3, and 0.5, respectively. The dashed lines are NLO + LO contributions, while the solid lines are only at LO. For illustration, we only show the case for $m_{A'}/m_\chi \simeq 2$ and $m_H = 0.1m_{A'}$. We see a clear dependence on the dark sector coupling α_D and differences between the NLO + LO and LO only contributions.

Also shown as the gray shaded region are the model independent constraints on this parameter space. Below ~10 MeV, there is a stringent bound from big bang nucleosynthesis and $\Delta N_{\rm eff}$, whereas the upper gray shaded region indicates bounds from a combination of direct detection experiments, including XENON1T, PANDAX, and SENSEI (obtained from Ref. [31]).

Similarly to the annihilation case above, we see the significance of the radiative corrections for different values of the ratio $m_H/m_{A'}$, particularly for large $m_{A'}/m_\chi$. For $m_H/m_{A'} \geq 1$ the effect of a heavy dark Higgs is decreased. As one decreases $m_H/m_{A'}$, we notice a significant correction to the total scattering cross section that increases as $m_{A'}/m_\chi$ rises, saturating for $m_{A'}/m_\chi \sim 5$.

V. DISCUSSION AND CONCLUSIONS

In this work, we revisit the computations for sub-GeV thermal dark matter processes. We consider a highly motivated and sought after scenario, in which (pseudo)-Dirac dark matter couples to the SM via a massive dark photon, representing a compelling benchmark model of dark matter. We focus on the corrections of order α_D, which is typically invoked to be large in order to obtain the observed relic density of the dark matter.

We compute the NLO corrections for thermal (pseudo-) Dirac dark matter annihilating in the early Universe, as this represents a very important target for upcoming experiments. We find that the NLO corrections can be quite significant, much larger than 10s of percents, depending on the $m_{A'}/m_\chi$ ratio, the mass of the dark Higgs and the strength of the dark sector coupling constant α_D. We find that this can result in a dramatic change compared to the targets inferred from tree-level calculations, as the mass of the Higgs in this model can be smaller compared to the mass of the dark photon. Hence it is an important result to establish the ability of proposed experiments to discover or constrain MeV scale dark matter, and to precisely quantify what we will learn from such experiments in the future. Furthermore, our results show that factorization into the "yield parameter" Y, as is common practice in the literature, can be misleading, especially in the resonance region, where the NLO corrections are more significant.

For completeness, we also show the direct detection limits based on DM-electron scattering. We find that the NLO corrections are as important as for the case of annihilation. One may wonder about the size of these corrections if the dark photon mass was generated through a different mechanism such as a Stueckelberg mass, and there were no dark Higgs particles. The scenarios for $m_H/m_{A'} \geq 1$ in the plots above correspond to this case. As we see, the corrections are still noticeable, though not as significant as those obtained for lighter Higgs masses. We leave a more dedicated study of pseudo-Dirac dark matter with larger mass splittings as well as other Lorentz structures of interest to future studies.

ACKNOWLEDGMENTS

We thank Basudeb Dasgupta for useful discussions. G. M. acknowledges support from the UC office of the President through the UCI Chancellor's Advanced Postdoctoral Fellowship. G. M. is also supported in part by the National Sciences and Engineering Research Council of Canada. T. M. P. T. and G. M. are supported in part by the U.S. National Science Foundation under Grant No. PHY-2210283. This work was performed in part at Aspen Center for Physics, which is supported by National Science Foundation Grant No. PHY-2210452.

APPENDIX A: DARK MATTER SELF-ENERGY

In terms of the Passarino-Veltmann scalar functions, the dark matter self-energy takes the form

$$\Sigma(p) = \frac{\alpha_D}{8\pi}\left[\frac{(\epsilon-2)\not{p}}{p^2}(A_0(m_{A'}^2) - A_0(m_\chi^2) + (-m_{A'}^2 + m_\chi^2 + p^2)B_0(p^2; m_{A'}^2, m_\chi^2)) - 2m_\chi(\epsilon-4)B_0(p^2; m_{A'}^2, m_\chi^2)\right], \quad \text{(A1)}$$

where $\not{p} \equiv \gamma^\mu p_\mu$ and $\epsilon = 4 - D$. The dark matter wave-function counterterm in the on-shell renormalization scheme, $\delta Z_2 = d\Sigma/d\not{p}, (\not{p} \to m_\chi)$, is given by

$$\delta Z_2 = -\frac{\alpha_D}{8\pi m_\chi^2}[(\epsilon-2)(m_{A'}^2(-B_0(m_\chi^2; m_{A'}^2, m_\chi^2)) + A_0(m_{A'}^2) - A_0(m_\chi^2)) + 2m_\chi^2(m_{A'}^2(\epsilon-2) - 4m_\chi^2)B_0{}'(m_\chi^2; m_{A'}^2, m_\chi^2)]. \quad \text{(A2)}$$

The dark matter mass counterterm in the on-shell scheme, $\delta m_\chi = \Sigma(p), (\not{p} \to m_\chi)$ can be similarly extracted, but does not enter into the computation of annihilation or scattering with electrons at NLO.

APPENDIX B: DARK PHOTON SELF-ENERGY

The tree-level dark photon propagator in the unitary gauge takes the form

$$iD_{\mu\nu}^{(0)}(k^2) = \frac{i(-g_{\mu\nu} + k_\mu k_\nu/m_{A'}^2)}{k^2 - m_{A'}^2}, \quad \text{(B1)}$$

where k is the momentum of the A'. The self-energy correction can be expressed as

$$\Pi_{\mu\nu}(k^2) \equiv g_{\mu\nu}\Pi_1(k^2) + k_\mu k_\nu \Pi_2(k^2), \quad \text{(B2)}$$

where the scalar function $\Pi_1(k^2)$ characterizes the transverse component and contributes to the S matrix, whereas the longitudinal component given by $\Pi_2(k^2)$ does not contribute when coupled to a conserved current. The mass counterterm for the massive dark photon is

$$\delta m_{A'}^2 = \mathrm{Re}[\Pi_1(m_{A'}^2)], \quad \text{(B3)}$$

and the wave function renormalization counterterm is

$$\delta Z_{A'} = Z_{A'} - 1 \simeq -\mathrm{Re}\left[\frac{d\Pi_1(m_{A'}^2)}{dk^2}\right], \quad \text{(B4)}$$

where $Z_{A'}$ is the wave function renormalization for a massive dark photon. The renormalized correction to the scalar part of the dark photon propagator is thus [51]

$$\Pi_{\mathrm{ren}}(k^2) = \Pi_1(k^2) - \delta m_{A'}^2 + (k^2 - m_{A'}^2)\delta Z_{A'}. \quad \text{(B5)}$$

We discuss the one-loop contributions from the dark matter and the dark Higgs to the dark photon self-energy separately, below. At NLO, these two classes of contributions are simply summed together.

1. Contribution from dark matter

Using dimensional regularization, the one-loop correction to $\Pi_1(k^2)$ with the DM fermion in the loop takes the following form:

$$\Pi_1(k^2) = \frac{\alpha_D}{2\pi(\epsilon-3)}((4m_\chi^2 - (\epsilon-2)k^2)B_0(k^2; m_\chi^2, m_\chi^2) + 2(\epsilon-2)A_0(m_\chi^2)), \tag{B6}$$

where $\epsilon = 4 - D$.

The dark matter contribution to the mass counterterm is

$$\delta m_{A'}^2 = \frac{\alpha_D}{2\pi(\epsilon-3)}\mathrm{Re}(2(\epsilon-2)A_0(m_\chi^2) + (4m_\chi^2 - m_{A'}^2(\epsilon-2))B_0(m_{A'}^2; m_\chi^2, m_\chi^2)) \tag{B7}$$

and the DM contribution to the wave function renormalization counterterm $\delta Z_{A'}$ is

$$\delta Z_{A'} = -\frac{\alpha_D}{2\pi(\epsilon-3)}\mathrm{Re}((\epsilon-2)B_0(m_{A'}^2; m_\chi^2, m_\chi^2) + (m_{A'}^2(\epsilon-2) - 4m_\chi^2)B_0{}'(m_{A'}^2; m_\chi^2, m_\chi^2)). \tag{B8}$$

2. Dark Higgs contribution

The one-loop correction $\Pi_1(k^2)$ to the dark photon self-energy due to dark Higgs is

$$\Pi_1(k^2) = \frac{\alpha_D q_\phi^2}{4\pi(\epsilon-3)k^2}\{(-2k^2(m_A^2(2\epsilon-5) + m_H^2) + k^4 + (m_A^2 - m_H^2)^2)B_0(k^2, m_A^2, m_H^2) + A_0(m_H^2)((5-2\epsilon)k^2 + m_A^2 - m_H^2) - A_0(m_A^2)(k^2 + m_A^2 - m_H^2)\}, \tag{B9}$$

where $\epsilon = 4 - D$. The contribution to the mass counterterm is

$$\delta m_{A'}^2 = \frac{\alpha_D q_\phi^2}{4\pi m_{A'}^2(\epsilon-3)}\mathrm{Re}\{(-4m_{A'}^4(\epsilon-3) - 4m_{A'}^2 m_H^2 + m_H^4)B_0(m_{A'}^2; m_{A'}^2, m_H^2) - A(m_H^2)(2m_{A'}^2(\epsilon-3) + m_H^2) + (m_H^2 - 2m_{A'}^2)A_0(m_{A'}^2)\} \tag{B10}$$

and the contribution to the wave function renormalization counterterm is

$$\delta Z_{A'} = \frac{\alpha_D q_\phi^2}{4\pi m_{A'}^4(\epsilon-3)}\mathrm{Re}\{m_H^2(m_H^2 - 2m_{A'}^2)B_0(m_{A'}^2; m_{A'}^2, m_H^2) + m_{A'}^2(4m_{A'}^4(\epsilon-3) + 4m_{A'}^2 m_H^2 - m_H^4)B_0'(m_{A'}^2; m_{A'}^2, m_H^2) + (m_H^2 - m_{A'}^2)A_0(m_{A'}^2) + (m_{A'} - m_H)(m_{A'} + m_H)A_0(m_H^2)\}. \tag{B11}$$

[1] Gianfranco Bertone and Tim M. P. Tait, A new era in the search for dark matter, Nature (London) **562**, 51 (2018).

[2] P. Cushman *et al.*, Working Group Report: WIMP Dark Matter Direct Detection, in *Snowmass 2013: Snowmass on the Mississippi* (2013); arXiv:1310.8327.

[3] Jodi Cooley *et al.*, Report of the topical group on particle dark matter for snowmass 2021, *Proceedings of the Snowmass 2021* (2022); arXiv:2209.07426.

[4] Pierre Fayet, Effects of the spin 1 partner of the Goldstino (gravitino) on neutral current phenomenology, Phys. Lett. B **95**, 285 (1980).

[5] Pierre Fayet, On the search for a new spin 1 boson, Nucl. Phys. **B187**, 184 (1981).

[6] Bob Holdom, Two U(1)'s and epsilon charge shifts, Phys. Lett. B **166**, 196 (1986).

[7] Eder Izaguirre, Gordan Krnjaic, Philip Schuster, and Natalia Toro, Testing GeV-scale dark matter with fixed-target missing momentum experiments, Phys. Rev. D **91**, 094026 (2015).

[8] Eder Izaguirre, Gordan Krnjaic, Philip Schuster, and Natalia Toro, Analyzing the discovery potential for light dark matter, Phys. Rev. Lett. **115**, 251301 (2015).

[9] Eder Izaguirre, Gordan Krnjaic, and Maxim Pospelov, MeV-scale dark matter deep underground, Phys. Rev. D **92**, 095014 (2015).

[10] Eder Izaguirre, Gordan Krnjaic, and Brian Shuve, Discovering inelastic thermal-relic dark matter at colliders, Phys. Rev. D **93**, 063523 (2016).

[11] Jonathan L. Feng and Jordan Smolinsky, Impact of a resonance on thermal targets for invisible dark photon searches, Phys. Rev. D **96**, 095022 (2017).

[12] Eder Izaguirre, Yonatan Kahn, Gordan Krnjaic, and Matthew Moschella, Testing light dark matter coannihilation with fixed-target experiments, Phys. Rev. D **96**, 055007 (2017).

[13] A. A. Aguilar-Arevalo *et al.* (MiniBooNE DM Collaboration), Dark matter search in nucleon, pion, and electron channels from a proton beam dump with MiniBooNE, Phys. Rev. D **98**, 112004 (2018).

[14] L. Marsicano, M. Battaglieri, M. Bondí, C. D. R. Carvajal, A. Celentano, M. De Napoli, R. De Vita, E. Nardi, M. Raggi, and P. Valente, Novel way to search for light dark matter in lepton beam-dump experiments, Phys. Rev. Lett. **121**, 041802 (2018).

[15] Asher Berlin and Felix Kling, Inelastic dark matter at the LHC lifetime frontier: ATLAS, CMS, LHCb, CODEX-b, FASER, and MATHUSLA, Phys. Rev. D **99**, 015021 (2019).

[16] Gopolang Mohlabeng, Revisiting the dark photon explanation of the muon anomalous magnetic moment, Phys. Rev. D **99**, 115001 (2019).

[17] Yu-Dai Tsai, Patrick deNiverville, and Ming Xiong Liu, Dark photon and muon $g-2$ inspired inelastic dark matter models at the high-energy intensity frontier, Phys. Rev. Lett. **126**, 181801 (2021).
[18] Michael Duerr, Torben Ferber, Christopher Hearty, Felix Kahlhoefer, Kai Schmidt-Hoberg, and Patrick Tunney, Invisible and displaced dark matter signatures at Belle II, J. High Energy Phys. 02 (2020) 039.
[19] Asher Berlin, Patrick deNiverville, Adam Ritz, Philip Schuster, and Natalia Toro, Sub-GeV dark matter production at fixed-target experiments, Phys. Rev. D **102**, 095011 (2020).
[20] Brian Batell, Jonathan L. Feng, Ahmed Ismail, Felix Kling, Roshan Mammen Abraham, and Sebastian Trojanowski, Discovering dark matter at the LHC through its nuclear scattering in far-forward emulsion and liquid argon detectors, Phys. Rev. D **104**, 035036 (2021).
[21] Brian Batell, Joshua Berger, Luc Darmé, and Claudia Frugiuele, Inelastic dark matter at the Fermilab short baseline neutrino program, Phys. Rev. D **104**, 075026 (2021).
[22] Mariana Carrillo González and Natalia Toro, Cosmology and signals of light pseudo-Dirac dark matter, J. High Energy Phys. 04 (2022) 060.
[23] C. Cazzaniga *et al.* (NA64 Collaboration), Probing the explanation of the muon (g-2) anomaly and thermal light dark matter with the semi-visible dark photon channel, Eur. Phys. J. C **81**, 959 (2021).
[24] Stefania Gori *et al.*, Dark sector physics at high-intensity experiments, arXiv:2209.04671.
[25] G. Krnjaic *et al.*, A snowmass whitepaper: Dark matter production at intensity-frontier experiments, arXiv:2207.00597.
[26] Martina Mongillo, Asli Abdullahi, Benjamin Banto Oberhauser, Paolo Crivelli, Matheus Hostert, Daniele Massaro, Laura Molina Bueno, and Silvia Pascoli, Constraining light thermal inelastic dark matter with NA64, Eur. Phys. J. C **83**, 391 (2023).
[27] Asli M. Abdullahi, Matheus Hostert, Daniele Massaro, and Silvia Pascoli, Semi-visible dark photon phenomenology at the GeV scale, Phys. Rev. D **108**, 015032 (2023).
[28] Nirmalya Brahma, Saniya Heeba, and Katelin Schutz, Resonant Pseudo-Dirac dark matter as a sub-GeV thermal target, Phys. Rev. D **109**, 035006 (2024).
[29] Timon Emken, Rouven Essig, Chris Kouvaris, and Mukul Sholapurkar, Direct detection of strongly interacting sub-GeV dark matter via electron recoils, J. Cosmol. Astropart. Phys. 09 (2019) 070.
[30] Itay M. Bloch, Andrea Caputo, Rouven Essig, Diego Redigolo, Mukul Sholapurkar, and Tomer Volansky, Exploring new physics with O(keV) electron recoils in direct detection experiments, J. High Energy Phys. 01 (2021) 178.
[31] Rouven Essig *et al.*, Snowmass2021 cosmic frontier: The landscape of low-threshold dark matter direct detection in the next decade, in *Snowmass 2021* (2022); arXiv:2203.08297.
[32] Haipeng An, Maxim Pospelov, Josef Pradler, and Adam Ritz, Directly detecting MeV-scale dark matter via solar reflection, Phys. Rev. Lett. **120**, 141801 (2018); **121**, 259903(E) (2018).
[33] Jae Hyeok Chang, Rouven Essig, and Samuel D. McDermott, Supernova 1987A constraints on sub-GeV dark sectors, millicharged particles, the QCD axion, and an axion-like particle, J. High Energy Phys. 09 (2018) 051.
[34] William DeRocco, Peter W. Graham, Daniel Kasen, Gustavo Marques-Tavares, and Surjeet Rajendran, Supernova signals of light dark matter, Phys. Rev. D **100**, 075018 (2019).
[35] Damiano F. G. Fiorillo and Edoardo Vitagliano, Self-interacting dark sectors in supernovae can behave as a relativistic fluid, Phys. Rev. Lett. **133**, 251004 (2024).
[36] Patrick J. Fitzpatrick, Hongwan Liu, Tracy R. Slatyer, and Yu-Dai Tsai, New thermal relic targets for inelastic vector-portal dark matter, Phys. Rev. D **106**, 083507 (2022).
[37] Cara Giovanetti, Mariangela Lisanti, Hongwan Liu, and Joshua T. Ruderman, Joint cosmic microwave background and big bang nucleosynthesis constraints on light dark sectors with dark radiation, Phys. Rev. Lett. **129**, 021302 (2022).
[38] Hooman Davoudiasl and William J. Marciano, Running of the U(1) coupling in the dark sector, Phys. Rev. D **92**, 035008 (2015).
[39] Aidan Reilly and Natalia Toro, Ultraviolet running constraints on low mass dark sectors, J. High Energy Phys. 01 (2024) 089.
[40] Tracy R. Slatyer, Indirect dark matter signatures in the cosmic dark ages. I. Generalizing the bound on s-wave dark matter annihilation from Planck results, Phys. Rev. D **93**, 023527 (2016).
[41] K. A. Olive (Particle Data Group), Review of particle physics, Chin. Phys. C **38**, 090001 (2014).
[42] Yonatan Kahn, Gordan Krnjaic, Nhan Tran, and Andrew Whitbeck, M^3: A new muon missing momentum experiment to probe $(g-2)_\mu$ and dark matter at Fermilab, J. High Energy Phys. 09 (2018) 153.
[43] Vladyslav Shtabovenko, Rolf Mertig, and Frederik Orellana, FeynCalc 9.3: New features and improvements, Comput. Phys. Commun. **256**, 107478 (2020).
[44] G. Passarino and M. J. G. Veltman, One loop corrections for e^+e^- annihilation into $\mu^+\mu^-$ in the Weinberg model, Nucl. Phys. **B160**, 151 (1979).
[45] T. Hahn and M. Perez-Victoria, Automatized one loop calculations in four-dimensions and D-dimensions, Comput. Phys. Commun. **118**, 153 (1999).
[46] Hiren H. Patel, Package-X 2.0: A Mathematica package for the analytic calculation of one-loop integrals, Comput. Phys. Commun. **218**, 66 (2017).
[47] Gary Steigman, Basudeb Dasgupta, and John F. Beacom, Precise relic WIMP abundance and its impact on searches for dark matter annihilation, Phys. Rev. D **86**, 023506 (2012).
[48] Ken'ichi Saikawa and Satoshi Shirai, Precise WIMP dark matter abundance and standard model thermodynamics, J. Cosmol. Astropart. Phys. 08 (2020) 011.
[49] N. Aghanim *et al.* (Planck Collaboration), Planck 2018 results. VI. Cosmological parameters, Astron. Astrophys. **641**, A6 (2020).
[50] Rouven Essig, Jeremy Mardon, and Tomer Volansky, Direct detection of sub-GeV dark matter, Phys. Rev. D **85**, 076007 (2012).
[51] Fred Jegerlehner, Renormalizing the standard model, Conf. Proc. C **900603**, 476 (1990).